DYNAMIC TOPOGRAPHY CHANGES OF SAND SPIT OF THE TENRYU RIVER MOUTH DUE TO OVERTOPPING WAVES

TOMOHIRO TAKAGAWA[1], YOSHIMITSU TAJIMA[1] HAIJIANG LIU[1], SATOSHI TAKEWAKA[2], SHINJI SATO[1]

1. *Department of Civil Engineering, The University of Tokyo, Hongo 7-3-1, Bunkyo-ku, Tokyo, 113-8656 Japan. takagawa@coastal.t.u-tokyo.ac.jp.*
2. *Department of Systems and Information Engineering, The University of Tsukuba, Tennodai 1-1-1, Tsukuba, Ibaraki, 305-8573 Japan. takewaka@kz.tsukuba.ac.jp.*

Abstract: In October 2009, the category-5 typhoon T0918 hit the Japan Pacific Coast and significant topographic changes occurred along the Enshu-nada coast due to the storm waves. The significant wave height was more than 10 m and rapid landward migration of the sand spit of the Tenryu river mouth was observed. Based on X-band radar image analysis, spatial and temporal changes of overtopping waves and corresponding sediment flux across the sand spit were revealed. Spatial concentration of the sediment flux can be explained by the nonlinear relationship between wave height of overtopping waves and corresponding sediment fluxes. A sediment flux model was developed based on the relationship. Maximum flux was estimated by the model to be 51 m^3/m/hour, which was achieved when high waves and high tide were observed simultaneously.

Introduction

Coastal topography changes rapidly due to storm waves. In October 2009, the category-5 Typhoon T0918 (Melor) hit the Japan Pacific Coast (Fig. 1). The central atmospheric pressure of the typhoon reached 910 hPa and maximum wind speed recorded 55 m/s. The Tenryu River mouth area, shown in Figure 1, is one of areas that suffered the most significant topographic changes due to T0918. The significant wave height marked more than 10 m (Fig. 2). The sand spit at the mouth of the Tenryu River migrated landward about 50 m (Fig. 3). From the viewpoint of coastal sediment management, it is very important to reveal the sediment movement and corresponding topographic change around the sand spits of river mouths, because the sand spit morphology affects both flow and wave fields and sediment movements (e.g. Tajima et al. 2011). However, observationally-based analysis of sediment movement is limited in such extreme wave event because of the difficulty of installation of observation equipments under high-energy conditions. In this study, a remote sensing technology of X-band radar was utilized for wave observation. Overtopping waves across the sand spit were successfully captured in the X-band radar observation. This study aims to establish a sediment transport model on overtopping waves across sand

spits or bars through the analysis of overtopping waves and topographic changes during the T0918 event.

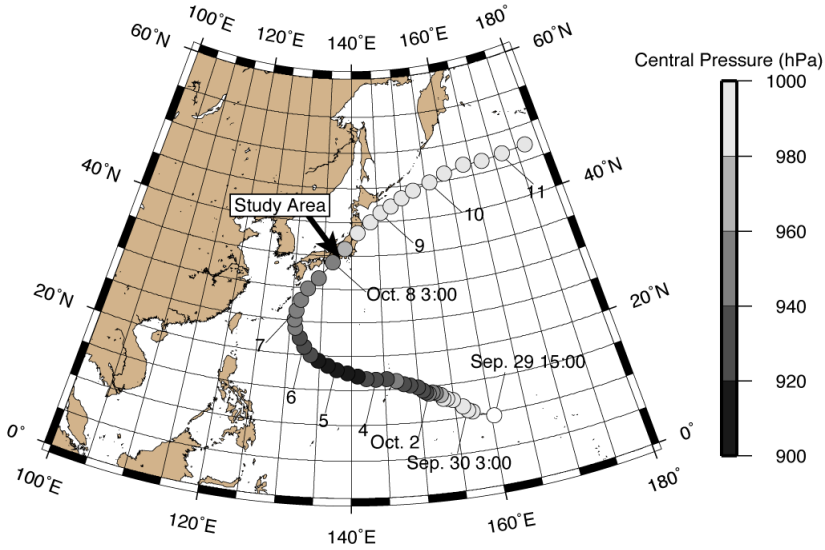

Fig. 1. The path of typhoon T0918 and the location of study area. The typhoon's positions every 3 hours are shown as circles. The gray scale indicates the central pressure of the typhoon.

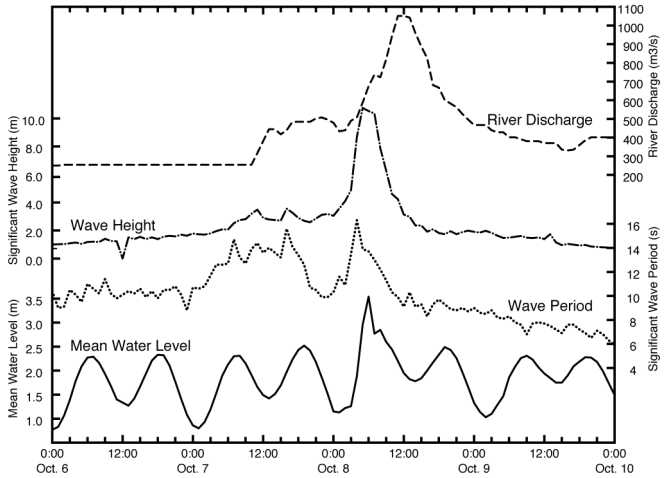

Fig. 2. Temporal changes of discharge of the Tenryu River, significant wave height, wave period and mean water level.

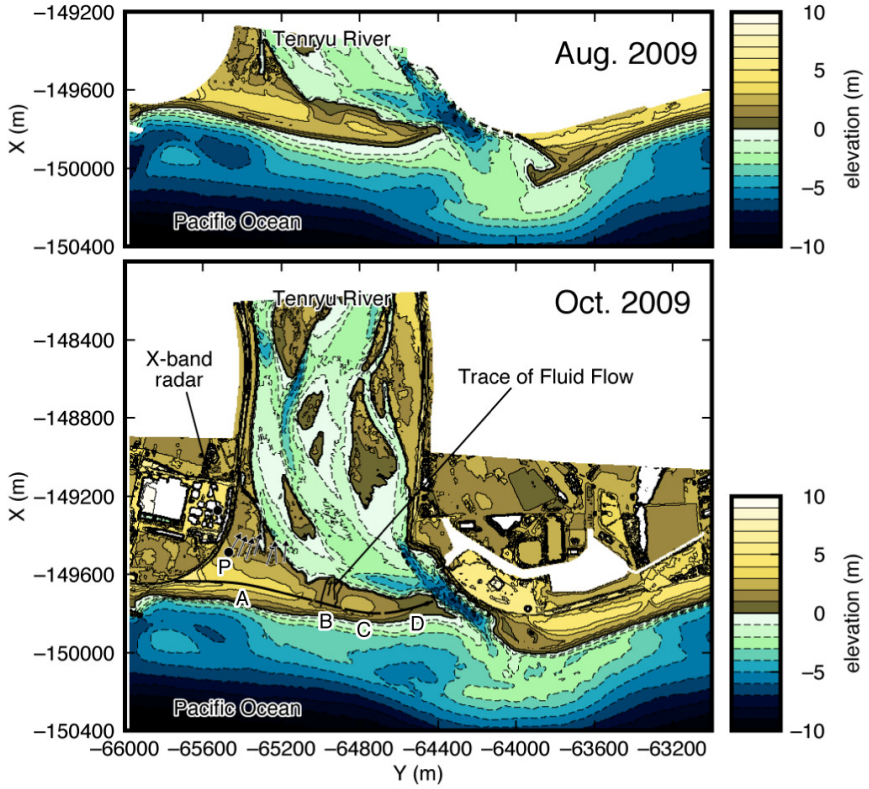

Fig. 3. Topographies around the Tenryu river mouth in August and October 2009. The arrows near the point P in the lower figure indicate the fallen directions of reed grasses shown in Fig. 4.

Topography Changes during T0918

Two topography data sets around the Tenryu River mouth were analyzed, one was measured in August, before the typhoon, and the other in October, just after the typhoon (Fig. 3). These data sets were obtained by the Ministry of Land, Infrastructure and Transport (MLIT), Japanese Government. Between August and October, no flood and high wave events happened except the T0918 event. Therefore, most of topographic changes between those data sets are thought to be caused by high waves generated by T0918. In the focusing area of 2.5×10^6 m^2 around the sand spit as shown in Figure 4, total budget of sediment volumetric change including void was 3.0×10^3 m^3. Sea-side of the spit was severely eroded, while the land-side of the spit and offshore of the eroded areas were accumulated. As a result of these sedimentation and erosion, the spit migrated about 50 m landward. No significant topographic changes were observed both in

the river area near the north end of the analyzed area and also in the offshore area deeper than −6 m T.P. Therefore, the sediment flux across the boundaries of focusing area is negligible. To capture the sediment movement over the spit, total increases of sediment volume along the landward part were calculated in each north-south section with 5 m intervals (Fig. 5). The boundary between landward and seaward parts is shown as the S−S' line in Figure 4. This boundary was set along the crest of sand spit in August 2009. Assuming zero sediment flux across the boundaries of the focusing area, sediment volume corresponding to the landward sand flux across the sand spit was obtained in each section. Total sediment volumes moved landward across the spit was estimated as 8.2×10^4 m^3. Alongshore distribution of landward sediment flux shows local concentration in the middle and east end of the spit (B and D sections in Fig. 5), where the crest height of the sand spit was lower than the other areas. This indicates that the sediment movement is strongly affected by the sand spit topography.

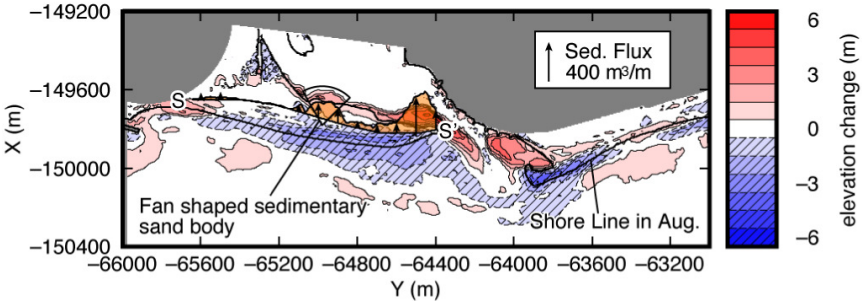

Fig. 4. Topography changes between August and October 2009. The arrows indicates estimated sediment fluxes across the crest of the sand spit.

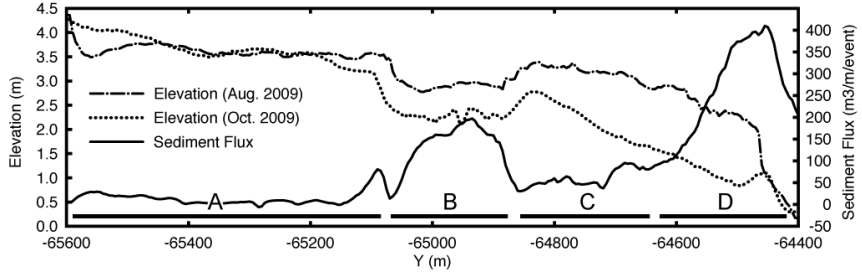

Fig. 5. The elevation change of the crest of sand spit between August and October 2009. The solid line indicates estimated sediment fluxes across the crest of the sand spit.

Overtopping Waves during T0918

Field survey was conducted just after the typhoon in order to capture the evidence of overtopped waves. Most of reed grasses fell down in landward direction in the north-west area of the sand spit (Fig. 6). This area was more than 200 m away from the shoreline, where moderate waves could not reach. The direction of reeds indicates the running direction of overtopping waves as shown in Fiture 3. Fan shaped over-wash sand sheet deposits were observed in west end and middle area (Fig. 4).

A X-band radar survey was also conducted during the storm event. The radar system has been installed on the rooftop of a building located at the right-side of the Tenryu River mouth (Fig. 3). The observation area is 5.3 km × 5.3 km. Radar echo signals were processed and recorded as an 8-bit gray image of 1024×1024 pixels (Fig. 7). It is known empirically that wave crests were shown as high-brightness lines in those images (Hasan & Takewaka, 2009). Image data were obtained every 2 seconds. The propagation of waves is observed from a sequence of radar images. Cross-shore time stack images were used to detect the overtopping waves. A typical time stack image is shown in Figure 7. The image shows temporal changes of a north-south section of radar images. Bright pixels moving northward with time indicates the motion of wave crests. In this figure, some wave crests stop in the sand spit area, while the others shown as arrows keep moving all over the area and reach the riverside of the spit. The later case is thought as an overtopping wave. In this way, overtopping waves were detected

Fig. 6. Reed grasses fell down in the north direction at the point of P in Fig.3. The broken line shows a front of sand-sheet deposits.

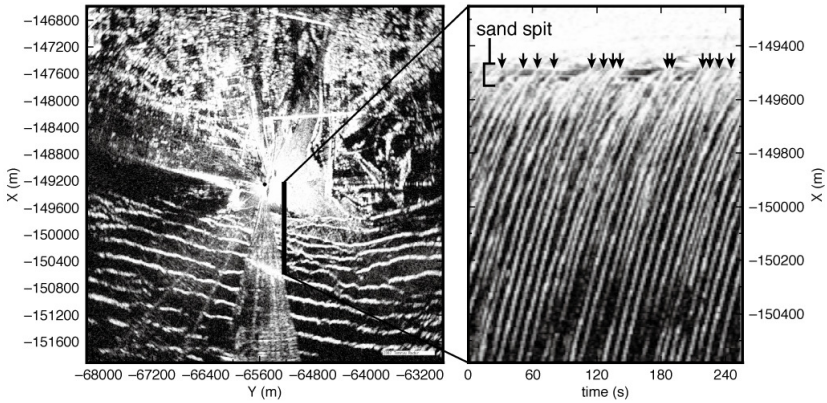

Fig. 7. X-band radar image (left) and cross-shore time stack image (right). Arrows show overtopping waves across the sand spit.

and counted manually by eyes in each north-south section with 50 m-intervals. Temporal and spatial changes of overtopping wave ratio were shown in Figure 8. The overtopping wave ratio P_e is defined as

$$P_e = N_e / N \tag{1}$$

where N_e is number of overtopping waves in a unit of time and N is number of incident waves in a unit of time. N_e was obtained by X-band radar analysis and N was calculated by the wave period data recorded at the Ryuyo wave gauge, about 1000m offshore from the river mouth with water depth of 40m.

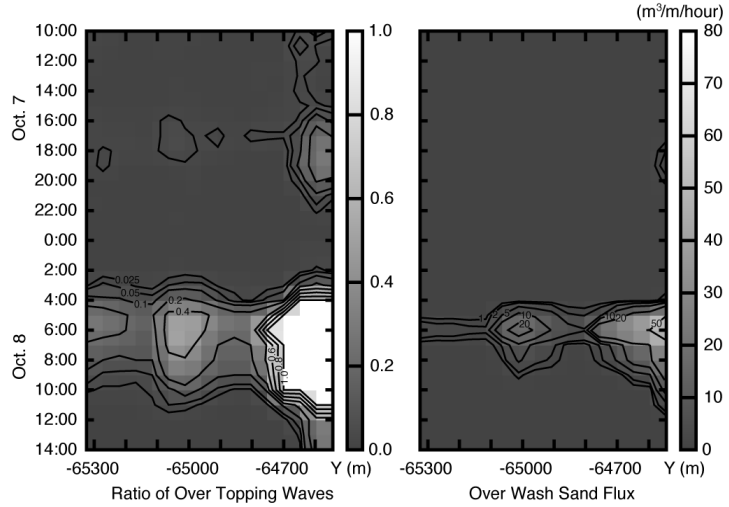

Fig. 8. Temporal and spatial changes of ratio of overtopping waves and over-wash sand flux estimated by the proposed model.

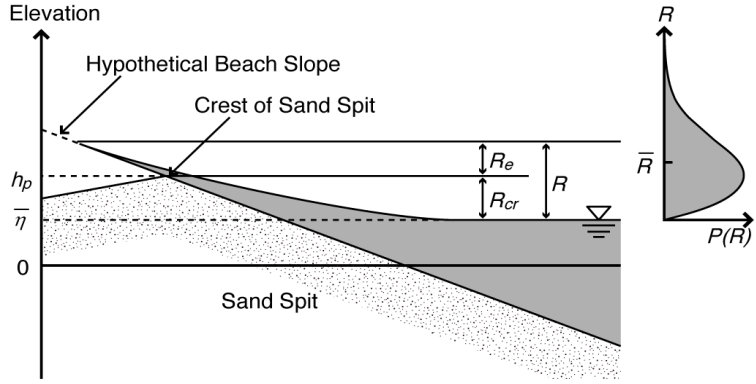

Fig. 9. Schematic diagram of model parameters.

Estimation of run-up heights

Parameters characterizing run-up and overtopping waves are shown in Figure 9. In order to simplify the treatment of wave height, hypothetical slope continuing upward beyond the crest of sand spit was assumed. Both of run-up and overtopping wave height were defined as the hypothetical run-up height on the hypothetical slope.

Based on field survey and laboratory observation on monochromatic waves (Hunt, 1959; Holman, 1986), wave run-up height R is typically parameterized as

$$R/H_0 = c\xi + d \tag{2}$$

where H_0 is the offshore wave height and c and d are dimensionless constants. ξ is a non-dimensional "surf similarity parameter" used in characterizing surf zone processes (Iribarren and Nogales, 1949) and is given by

$$\xi = \tan\beta \Big/ \sqrt{H_0/L_0} \tag{3}$$

where $\tan\beta$ is the beach slope, L_0 is the deep water wave length defined as $L_0 = gT_s^2/2\pi$ by linear theory, g is the gravity acceleration, and T_s is the significant wave period.

Assuming that the probability density distribution of incident wave height follows Rayleigh distribution and surf similarity parameter does not vary with

individual wave properties, the probability density distribution of run-up height also follows Rayleigh distribution and is given as

$$P(R) = \frac{\pi}{2}\frac{R}{\overline{R}^2}\exp\left(-\frac{\pi}{4}\left(\frac{R}{\overline{R}}\right)^2\right) \quad (4)$$

where $\overline{R}$ is the average of R. Then the probability P_e of R exceeding R_{cr} is given by

$$P_e = \int_{R_{cr}}^{\infty} P(R)dR = \exp\left(-\frac{\pi}{4}\left(\frac{R_{cr}}{\overline{R}}\right)^2\right) \quad (5)$$

where R_{cr} is the critical run-up height for over-wash event. R_{cr} is given by $R_{cr} = h_c - \overline{\eta}$, where h_c is the height of the sand spit crest and $\overline{\eta}$ is the mean water level. Here the average height of sand spit crests on August and October 2009 in each alongshore point was used as h_c. $\overline{\eta}$ was obtained from Ryuyo wave gauge data.

Empirical parameters c and d can be determined by using the least square method to minimize the difference between the P_e obtained by using Eq. 1 and the P_e calculated by using Eqs. 2, 3, and 5. Once these parameters were determined, $\overline{R}$ can be evaluated only from wave gauge data and topography data of sand spit. However, large value of P_e is problematic because $\overline{R}$ will reach an infinite value when P_e comes close to 1. In this procedure, it is difficult to estimate reliable value of $\overline{R}$ when P_e is close to 1. Furthermore, it is also difficult to count overtopping waves in X-band time stack images when P_e is more than 0.5. In such case, overlaps of waves happen frequently and it is hard to distinguish individual incident waves in surf zone. Therefore, $\overline{R}$ was decided to estimate by empirical extrapolation on the basis of the relationship between $\overline{R}$ and H_0 when P_e is more than 0.5. The relationship is shown in Figure 10. The data was selected in the smaller P_e case. Finally, an empirical relationship was obtained by the least square method as follows:

$$\overline{R} = 0.101H_0 + 0.514 \quad (6)$$

where the unit of $\overline{R}$ and H_0 is in meter. This empirical formula was used to estimate $\overline{R}$ when P_e is more than 0.5. This estimation was applied for only 7 % of all data in this study.

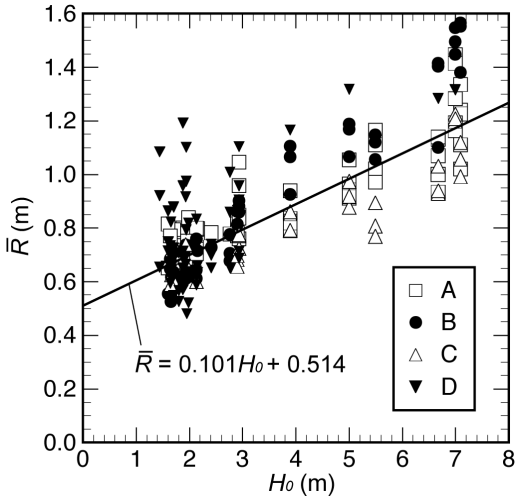

Fig. 10. Relationship between H_0 and $\overline{R}$. A-D indicate the data from A-D section of Figure 3.

Sediment transport model on overtopping waves

Sediment flux q is usually modeled in the power model as a product of flow velocity and bottom shear stress. Bottom shear stress for rough turbulent flow is proportional to the square of flow velocity. The flow velocity at the crest of sand spit is thought to be proportional to the square root of excess run-up height $R_e = R - R_{cr}$ because the run-up wave motion on an uniform slope is well approximated by parabolic motion (e.g. Shen & Meyer, 1963; Roberts et al, 2010). Therefore, the following relation is assumed.

$$q \propto R_e^{\frac{3}{2}} \tag{7}$$

Therefore, sediment flux was modeled as

$$q \propto \kappa R_e^{\gamma} \tag{8}$$

where κ and γ are regression coefficients. γ was expected close to 1.5. According to Eq. 8, the total landward over-wash sediment flux at each point of sand spit crest during the typhoon event is given by

$$Q_{\text{model}} = \int \int_0^{\infty} \kappa R_e^{\gamma} \cdot P\left(R_{cr} + R_e\right) \cdot N dR_e dt \tag{9}$$

The regression coefficients were estimated by the least square method so that the difference between the total sediment flux $Q_{\text{measurement}}$ obtained by the

topographic analysis and the total sediment flux Q_{model} evaluated by the proposed model. The estimated value of κ and γ are 0.0911 and 1.71, correspondingly. The value of γ is near to the expected value of 1.5. The relationship $Q_{measurement}$ and Q_{model} is shown in Figure 11. They are well correspondent with each other.

Figure 8 shows temporal and spatial changes of over-wash sediment flux estimated by the proposed model. As shown in Figure 8, Sediment flux distribution was more concentrated both spatially and temporally than the ratio of overtopping waves. According to the model, maximum flux was estimated to be about 51 m^3/m/hour. Over 70 % of total volume of sand transportation during the typhoon was transported within 4 hours around 5 a.m. on October 8 when high waves and high tide were observed simultaneously. Therefore, over-washed sediment motion generated by overtopping waves across a sand spit is found to be highly concentrated phenomena both temporally and spatially.

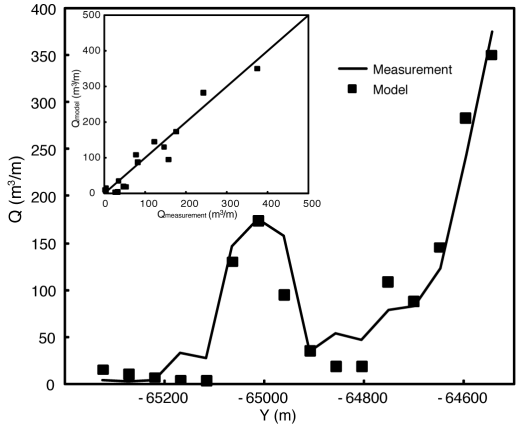

Fig. 11. Comparison between the sediment flux $Q_{measurement}$ and Q_{model}.

Horizontal distribution of wave field

On the analysis above, alongshore variation of wave field was neglected to simplify the phenomena. To capture the alongshore variability, Figure 10 was examined again here. In this figure, $\overline{R}$ of sections B and D shows larger value than A and C. This implies that other factors neglected in the proposed model still affect the run-up heights. Alongshore variation of wave field is thought to be one of those factors because $\overline{R}$ is related with alongshore location.

To examine alongshore variation of wave field, a sequence of X-band radar images at 5 a.m. on Oct. 8 was analyzed by using Particle Image Velocimetry

(PIV) technique. Horizontal wave celerity field obtained by PIV is shown in Figure 12. Arrows show local concentration of waves around sections B and D. These local concentrations are thought to be caused by wave refraction which is related to topography and wave-current interaction. These alongshore effects should be counted in sediment transport analysis to improve the model.

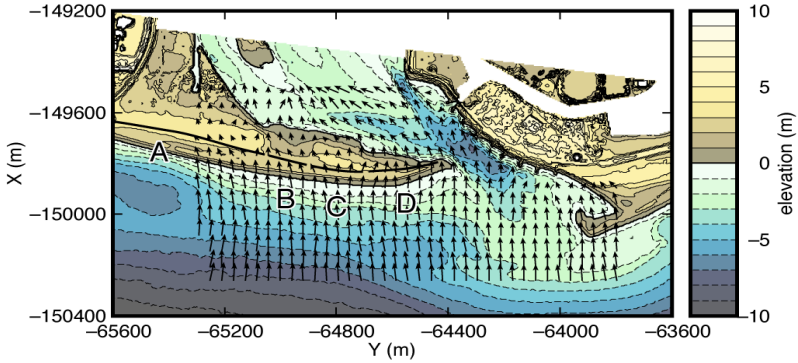

Fig. 12. Wave celerity distribution on October 8 at 5:00 a.m.

Conclusions

Local concentration of sediment transport across the sand spit was observed in a field survey and topography data analysis. Based on X-band radar image analysis, spatial and temporal changes of overtopping waves and corresponding sediment flux across the sand spit were revealed. Sediment flux distribution was more concentrated both spatially and temporally than the ratio of overtopping waves. A sediment transport model on overtopping waves across sand spits was established in this study. The model parameters are empirically estimated on the basis of observation data analysis. According to the model, maximum flux was estimated to be about 51 m^3/m/hour. Over 70 % of total volume of sand transportation during the typhoon was transported within 4 hours around 5 a.m. on October 8 when high waves and high tide were observed simultaneously.

Acknowledgements

This study is a part of Tenryu-Enshunada Project, “Dynamic sediment management and coastal disaster prevention by advanced technologies” supported by the Special Coordination Funds for promoting Science and Technology of Ministry of Education, Culture, Sports, Science and Technology, Japan. Authors would like to appreciate to Ministry of Land, Infrastructure, Transport and Tourism for wave and topography data.

References

Hasan, G.M.J. and S. Takewaka (2009). "Wave run-up analyses under dissipative condition using X-band radar," *Coastal Engineering Journal*, 51 (2), 177-204.

Holman, R.A. (1986): Extreme value statistics for wave run-up on a natural beach, *Coastal Engineering*, Vol. 9, pp. 527-544.

Hunt, I.A. (1959). "Design of Seawalls and Breakwaters," *J. Waterway and Harbors*, 85, 123-152.

Iribarren, C.R. and C. Nogales (1949). "Protection des ports," *XVIIth International Naval Congress*, Lisbon, Portugal, 31-80.

Longuet-Higgins, M.S. (1952): On the statistical distribution of the heights of sea waves, *J. Marine Research*, Vol. 3, pp. 245-266.

Roberts, T.M., P. Wang and N.C. Kraus (2010): Limits of wave runup and corresponding beach-profile change from large-scale laboratory data, *J. Coastal Research*, Vol. 26, pp. 184-198.

Shen, M.C. and R.E. Meyer (1963): Climb of a bore on a beach, Part 3: Run-up, *Journal of Fluid Mechanics*, Vol. 16, pp. 113-125.

Tajima, Y., H. Liu, T. Takagawa and S. Sato (2011). "Selective movements of sand and gravels and resulting dynamic morphology changes observed around the Tenryu River mouth," *Int. Conf. on Coastal Sediments*.